Exploration Geophysics (2006) 37, 239–244

Efficient 3D electromagnetic modelling in the presence of anisotropic conductive media, using integral equations

Sheng Fang[1] **Guo-zhong Gao**[2] **Carlos Torres-Verdín**[2]

Key Words: electromagnetic, numerical simulation, integral equation, anisotropy, induction tool

ABSTRACT

We present a novel technique to simulate numerically the measurements performed by a borehole induction-logging tool in 3D anisotropic rock formations. The simulations are based on an integral equation formulation. Previously, such a formulation was considered impractical for solving large-scale problems due to the resulting large full matrix. To overcome this difficulty, we assume a uniform background model and make use of a uniform grid whereupon there is no need to construct explicitly all of the entries of the full Green's function matrix.

Using a uniform background model, the entries of the corresponding electric and magnetic Green's tensors are relatively easy to calculate. In the presence of a uniform grid (not necessarily cubic), it is only necessary to calculate the first row of the resulting electric Green's function matrix. Further, because the matrix is block Toeplitz, it can be rewritten into a block circulant form, and therefore matrix-vector multiplication can be efficiently performed with two FFTs and one inverse FFT. This strategy reduces the computation cost from $\mathbf{O}(N\times N)$ to $\mathbf{O}(N\times log^2 N)$. In addition to the substantial computer savings, the FFT technique also substantially reduces memory storage requirements because only the first row and the first column in the block Toeplitz matrix are needed to perform the computations of the remaining entries of the matrix.

Numerical simulations of the measurements performed with an induction tool in dipping and anisotropic rock formations are benchmarked against accurate 3D finite-difference and 1D codes. These benchmark exercises show that the newly developed integral-equation algorithm produces accurate and efficient simulations for a variety of borehole and formation conditions.

INTRODUCTION

The advent of a commercial electromagnetic (EM) multi-component borehole logging tool with capabilities to measure electric anisotropy, has spearheaded efforts to simulate numerically the tool's response in complex 3D logging environments (Wang and Fang, 2001; Avdeev et al., 2002; Newman and Alumbaugh, 2002). Modelling formation electric anisotropy effects is of significance to the accurate petrophysical interpretation of induction logging tool responses and to date remains an open challenge (Moran and Gianzero, 1979; Klein, et al., 1997; Gianzero, 1999; Kriegshauser et al., 2000).

[1] *Baker Atlas*
2001 Rankin Rd
Houston, TX, 77073,USA
Email: sheng.fang@bakeratlas.com

[2] *Dept. of Petroleum and Geosystems Engineering*
The University of Texas at Austin
Austin, Texas, 78712, USA

Presented at the 3DEM III Workshop, February 2003, Adelaide. This version received 11 May, 2006.

So far, both finite difference (FD) and integral equation (IE) approaches have been developed to solve a general full 3D anisotropic problem. The FD approach is flexible in handling the complexity of formation models but is time consuming in solving problems with fine structures (Wang and Fang, 2001; Newman and Alumbaugh, 2002). On the other hand, the IE method is perfect for solving a small-scale problem. For a large-scale problem, the IE approach is usually considered inefficient because of the associated computer expenses in solving a large and full stiffness matrix. However, recent developments suggest that the IE method could also be used for the solution of large-scale problems within reasonable computer resources (Gan and Chew, 1994; Liu et al., 2001; Avdeev et al., 2002; Hursan and Zhdanov, 2002). Moreover, the IE approach has the advantage to yield an approximation that is exceedingly faster to compute than with alternative finite-difference approaches (e.g., Born, 1933; Habashy et al., 1993; Zhdanov and Fang, 1996; Fang and Wang, 2000; Gao et al., 2003). In this paper, we describe yet novel developments on the IE approach and their application to simulate the response of a borehole induction tool in the presence of anisotropic formations.

Integral equation techniques require of the calculation of a dyadic Green's function for an assumed background model and entail the solution of a full matrix linear equation resulting from the discretisation of the anomalous scattering medium (anomalous domain). The background model can be chosen arbitrarily as long as the Green's function remains amenable to efficient computations. In subsurface geophysical applications, a layer background is usually assumed for the computation of the Green's functions (e.g., Hohmann, 1983; Wannamaker et al., 1983; Xiong, 1992; Avdeev et al., 2002). The integral equation approach becomes less efficient when the number of cells used in the discretisation of the anomalous domain is relatively large. A large number of cells substantially increase both the computation time required to solve the large full matrix equation and the memory required for storage. In the paper of Xiong and Tripp (1995), a block system iteration method was used to solve the linear-system equation. This extends the capability of the IE method to deal with large problems. However, the problem size still remains very limited. The overall computational complexity was measured at $\mathbf{O}(N\times N)$, where N is the total number of cells in the calculation. The memory requirement was roughly $\mathbf{O}(N\times N)$ bytes. On the other hand, Avdeev et al. (2002) and Hursan and Zhdanov (2002) reported a CG-FFT (Conjugate Gradient - Fast Fourier Transform) approach (Catedra et al., 1995) to perform the computations. The CG-FFT method can achieve the computation complexity of $\mathbf{O}(N\times log^2 N)$. However, in these papers FFT techniques were applied in the horizontal directions only because of the assumption of a layer background. The overall computational complexity was of the order of $\mathbf{O}(N_x\times N_y\times N_z\times N_z\times log_2 N_x\times log_2 N_y)$, where N_x, N_y, and N_z are the number of cells in each coordinate direction, respectively. The reported memory size was roughly $\mathbf{O}(N_x\times N_y\times N_z\times N_z)$ bytes. This approach is efficient when N_z is small. In well logging applications, this is not the case. Moreover, the time required for the calculation of the Green's function becomes critical when N_z is large.

In order to make efficient use of the properties of the CG-FFT approach, which entails a computational complexity of the order

of $O(N \times log_2 N)$, the FFT technique needs to be applied in all three coordinate directions. The same approach has been used to solve scattering problems in the presence of an isotropic formation by Gan and Chew (1994), and Liu et al. (2001). However, to date there are no equivalent algorithms reported in the open technical literature to solve a full 3D anisotropy diffusion problem. In this paper, we apply the CG-FFT type method to simulate the response of an induction borehole tool response in the presence of dipping and anisotropic rock formations. To this end, a uniform isotropic formation background model is used and the anomalous domain is uniformly discretised in each coordinate direction. Such a strategy requires of the explicit calculation and memory storage of only the first row of the associated electric Green's function matrix, thereby substantially improving the efficiency of the algorithm. Likewise, presence of anisotropy in the scattering medium can be easily handled using the same technique – average effective conductivity – presented in the paper by Wang and Fang (2001).

The accuracy and the speed of the newly developed algorithm mainly depend on the grid size, which in turn is controlled by both detailed formation structure and tool configurations. For the examples described in this paper (128×64×128 grid size), it takes about 40 minutes of a SUN Workstation's CPU time (900 MHz floating-point processor) to produce accurate solutions for a single logging tool position.

NOMENCLATURE

σ'	Ohmic conductivity
ε_0	electrical permittivity of free space.
ε_r	dielectric constant.
μ_0	magnetic permeability of free space.
ω	angular frequency ($2\pi f$).
$i = \sqrt{-1}$	
t	time
$e^{-i\omega t}$	time convention
$\sigma = \sigma' - i\omega\varepsilon_r\varepsilon_0$	
$\mathbf{r} = (z,y,x)$	Cartesian coordinates, equivalent to $x\hat{\mathbf{x}} + y\hat{\mathbf{y}} + z\hat{\mathbf{z}}$.
T	superscript, denotes transpose.
=	denotes a 3×3 tensor.
H_{xy}	magnetic field generated in x-direction by a y-directed source (the second subscript represents the source direction).

INTEGRAL EQUATION METHOD

Basic Equations

Following the paper of Hohmann (1983), the integral equations for electric and magnetic fields can be written as

$$\mathbf{E}(\mathbf{r}) = \mathbf{E}_b(\mathbf{r}) + \int_\tau \bar{\bar{G}}^e(\mathbf{r},\mathbf{r}_0)\cdot\Delta\bar{\bar{\sigma}}\cdot\mathbf{E}(\mathbf{r}_0)d\mathbf{r}_0 \ , \qquad (1)$$

and

$$\mathbf{H}(\mathbf{r}) = \mathbf{H}_b(\mathbf{r}) + \int_\tau \bar{\bar{G}}^h(\mathbf{r},\mathbf{r}_0)\cdot\Delta\bar{\bar{\sigma}}\cdot\mathbf{E}(\mathbf{r}_0)d\mathbf{r}_0 \ , \qquad (2)$$

where $\mathbf{E}(\mathbf{r})$ and $\mathbf{H}(\mathbf{r})$ are the electric and magnetic fields, respectively, and $\mathbf{r}$ is the location vector. $\mathbf{E}_b(\mathbf{r})$ and $\mathbf{H}_b(\mathbf{r})$ are the electric and magnetic fields, respectively, associated with a background medium of dielectric constant ε_{rb} and Ohmic conductivity σ_b', at location $\mathbf{r}$. Accordingly, the background's complex conductivity is given by $\sigma_b = \sigma_b' - i\omega\varepsilon_{rb}\varepsilon_0$ (time harmonic, $e^{-i\omega t}$). At low frequencies, the expression for the background conductivity simplifies to $\sigma_b = \sigma_b'$.

In general, the background model can be arbitrarily chosen as long as the Green's function can be calculated in an efficient and expeditious manner. In the method proposed in this paper, the simplest possible choice is made, i.e., that of a homogeneous, unbounded, and isotropic background model. The reasons for such a choice are: (1) the Green's functions and background fields can be calculated in a very efficient manner, (2) the complexity of electrical anisotropy does not need to be considered at this stage, and (3) many special features ensue as the result of using uniform grids in constructing the numerical integral equation matrix.

Green's Function

The electric Green's tensor included in equations (1) and (2) can be expressed in closed form as

$$\bar{\bar{G}}^e(\mathbf{r},\mathbf{r}_0) = \left(i\omega\mu_0\bar{\bar{\mathbf{I}}} + \frac{1}{\sigma_b}\nabla\nabla\right)g(\mathbf{r},\mathbf{r}_0) \ , \qquad (3)$$

where μ_0 is free space magnetic permeability, the scalar function $g(\mathbf{r},\mathbf{r}_0)$ satisfies the wave equation

$$\nabla^2 g(\mathbf{r},\mathbf{r}_0) + k_b^2 g(\mathbf{r},\mathbf{r}_0) = -\delta(\mathbf{r}-\mathbf{r}_0) \ , \qquad (4)$$

whose solution can be explicitly written as

$$g(\mathbf{r},\mathbf{r}_0) = \frac{e^{ik_b|\mathbf{r}-\mathbf{r}_0|}}{4\pi|\mathbf{r}-\mathbf{r}_0|} = \frac{e^{ik_b R}}{4\pi R} \ , \qquad (5)$$

where $k_b^2 = i\omega\mu_0\sigma_b$.

The magnetic Green's tensor is related to the electric Green's tensor through the expression

$$\bar{\bar{G}}^h(\mathbf{r},\mathbf{r}_0) = \frac{1}{i\omega\mu_0}\nabla\times\bar{\bar{G}}^e(\mathbf{r},\mathbf{r}_0) \ . \qquad (6)$$

Finally, the tensor $\Delta\bar{\bar{\sigma}} = \bar{\bar{\sigma}} - \sigma_b\bar{\bar{\mathbf{I}}} = \Delta\bar{\bar{\sigma}}' - i\omega\mu_0\Delta\varepsilon_r\varepsilon_0\bar{\bar{\mathbf{I}}}$ is the complex conductivity contrast within scatterers, where $\Delta\varepsilon_r = \varepsilon_r - \varepsilon_{rb}$, $\Delta\bar{\bar{\sigma}}' = \bar{\bar{\sigma}}' - \sigma_b'\bar{\bar{\mathbf{I}}}$ and $\bar{\bar{\mathbf{I}}}$ is the identity matrix.

Numerical Solution

Equations (1) and (2) are Fredholm integral equations of the second kind. A solution of these equations can be obtained using the method of moments (MoM). By discretising equation (1) in the anomalous domain and by assuming the field quantities in each cell as constant, we can obtain the full matrix equation:

$$(\bar{\bar{\mathbf{I}}} - \bar{\bar{\bar{G}}}\bar{\bar{\bar{\Delta\sigma}}})\mathbf{E}_a = \bar{\bar{\bar{G}}}\bar{\bar{\bar{\Delta\sigma}}}\mathbf{E}_b \ , \qquad (7)$$

where $\bar{\bar{\bar{G}}}$ is the tensor Green's function matrix, $\bar{\bar{\bar{\Delta\sigma}}}$ is an anomalous tensor conductivity matrix that can be computed using the technique described in Wang and Fang (2001), $\mathbf{E}_a$ ($= \mathbf{E} - \mathbf{E}_b$) is an anomalous electric field vector, $\mathbf{E}$ is the total electric field vector, and $\mathbf{E}_b$ is the normal field vector consistent with the assumed background model.

Solving equation (7) involves the following difficulties for large-scale problems: (a) matrix filling time is substantial, (b) very large memory storage, and (c) time-consuming solution of the complex linear system. For a large-scale 3D problem, often the solution to EM scattering cannot be obtained with a direct method. For instance, in a case of 1 million discretisation cells, 0.2 CPU seconds are needed to compute 10 000 entries (each entry is a 3 by 3 tensor) of the linear-system matrix. It will take approximately 231 days to compute the entries of the full matrix without solving it. The memory requirement is also critical. For the above hypothetical case, more than 33 gigabytes of memory are needed if every entry is kept in static memory.

Obviously, such requirements place rather impractical constraints to most of today's computer platforms.

However, there is no need to calculate all entries in the MoM's linear-system matrix when the grid is uniform in each coordinate direction. Due to the fact that the Green's tensor and its volume integration depend only on the relative position of a given pair of cells, only the entries of the first row are needed to perform the calculations. The remaining entries can be substituted and sign adjusted from the entries of the first row. This strategy entails a computation approximately 100 times faster than the direct calculation. In the above scenarios, if every entry must be accessed, the matrix filling time would still be more than two days. Fortunately, by further studying the symmetry properties of the Green's tensor matrix, it can be shown that the matrix actually exhibits a block Toeplitz form. Toeplitz matrices possess several unique properties. First, Toeplitz matrices have a constant diagonal and can be fully described by their first row and first column:

$$\bar{\bar{\mathbf{T}}} = \begin{bmatrix} t_0 & t_{-1} & t_{-2} & \cdots & t_{-(n-1)} \\ t_1 & t_0 & t_{-1} & \cdots & \\ t_2 & t_1 & t_0 & \cdots & \vdots \\ \vdots & \vdots & \vdots & \ddots & \\ t_{n-1} & & \cdots & & t_0 \end{bmatrix}. \tag{8}$$

In this sense, it can be said that a Toeplitz matrix resembles a sparse system. Thus the storage can be dramatically reduced. Second, Toeplitz matrices can be easily transformed into their kin matrices – circulant matrices (Golub and Van Loan, 1996, page 201), with the associated Toeplitz matrix embedded in the circulant matrix, i.e.,

$$\bar{\bar{\mathbf{T}}} = \begin{bmatrix} \bar{\bar{\mathbf{T}}} & * \\ * & * \end{bmatrix}. \tag{9}$$

Explicitly, the circulant matrix has the form:

$$\bar{\bar{\mathbf{C}}} = \begin{pmatrix} c_0 & c_{n-1} & c_{n-2} & \cdots & c_1 \\ c_1 & c_0 & c_{n-1} & \cdots & c_2 \\ c_2 & c_1 & c_0 & \cdots & c_3 \\ \vdots & \vdots & \vdots & & \vdots \\ c_{n-1} & c_{n-2} & c_{n-3} & \cdots & c_0 \end{pmatrix}. \tag{10}$$

The first column of the circulant matrix is composed of the elements of the first column $\mathbf{t}_{col} = [t_0\, t_1 \cdots t_{n-1}]^{\mathrm{T}}$ and the reverse arrangement of the first row $\mathbf{t}_{row} = [t_{-(n-1)}\, t_{-(n-2)} \cdots t_{-1}]^{\mathrm{T}}$ of the associated Toeplitz matrix $\bar{\bar{\mathbf{T}}}$, i.e.,

$$\mathbf{c} = \begin{pmatrix} \mathbf{t}_{col} \\ \mathbf{0} \\ \mathbf{t}_{row} \end{pmatrix}, \tag{11}$$

where zeros are added to make the dimension of $\mathbf{c}$ equal to an integer power of 2. The circulant matrix can be formed using $\mathbf{c}$ and the identity matrix, namely,

$$\bar{\bar{\mathbf{C}}} = \begin{pmatrix} \mathbf{c} & \mathbf{Rc} & \mathbf{R}^2\mathbf{c} & \cdots & \mathbf{R}^{n-1}\mathbf{c} \end{pmatrix}, \tag{12}$$

where $\mathbf{R} = \begin{pmatrix} \mathbf{e}_2 & \mathbf{e}_3 & \cdots & \mathbf{e}_n & \mathbf{e}_1 \end{pmatrix}$ and $\mathbf{e}_k$ is the k-th column of the identity matrix.

An important property of the circulant matrix is that the multiplication of a circulant matrix and a vector can be performed using the FFT. In equation form:

$$\mathbf{y} = \bar{\bar{\mathbf{C}}}\mathbf{x} = \mathrm{ifft}\left(\mathrm{fft}(\mathbf{c}) * \mathrm{fft}(\mathbf{x})\right), \tag{13}$$

where $\mathbf{c}$ is the first column of the circulant matrix, and * stands for element-wise multiplication.

Thus, if an iterative method is used to solve the linear system, then the matrix-vector multiplications $\bar{\bar{G}} \cdot \left(\overline{\overline{\Delta\sigma}}\mathbf{E}_a\right)$ and $\bar{\bar{G}} \cdot \left(\overline{\overline{\Delta\sigma}}\mathbf{E}_b\right)$ in equation (7) can be performed using the FFT. Consequently, only the first row and the first column are needed in the tensor Green's function matrix to perform such an operation. This approach also substantially reduces memory storage requirements and the CPU time required for the calculation of the entries of $\bar{\bar{G}}$ is much less than the time otherwise required to compute all the entries separately.

Note that the use of the FFT requires that the vector be expanded to a length equal to an integer power of 2 with zeros according to the dimension of $\mathbf{c}$, namely,

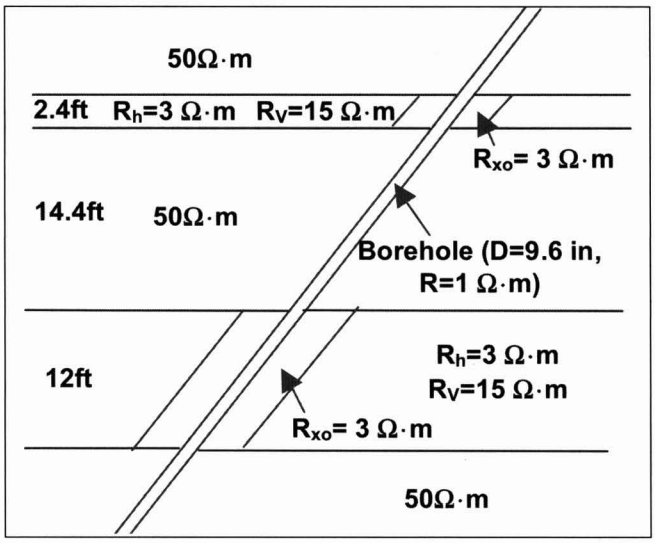

Fig. 1. Diagram showing a 5-layer electrical conductivity model and associated geometrical dimensions (not to scale).

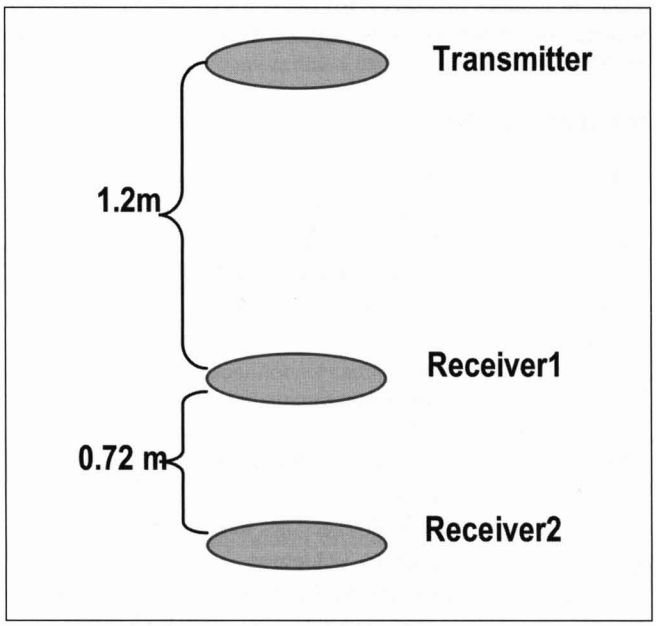

Fig. 2. Assumed tool configuration for borehole induction logging (not to scale).

$$\mathbf{x}' = \begin{pmatrix} \mathbf{x} \\ \mathbf{0} \end{pmatrix}, \tag{14}$$

$$\mathbf{y}' = \overline{\overline{\mathbf{C}}}\mathbf{x}' = \begin{pmatrix} \overline{\overline{\mathbf{T}}} & * \\ * & * \end{pmatrix}\begin{pmatrix} \mathbf{x} \\ \mathbf{0} \end{pmatrix} = \begin{pmatrix} \overline{\overline{\mathbf{T}}}\mathbf{x} \\ * \end{pmatrix}. \tag{15}$$

The final solution is the top n elements in y'.

By making use of the FFT the computation cost can be reduced from $\mathbf{O}(N^2)$ to $\mathbf{O}(N \times log_2 N)$. For large N, the time savings can be substantial.

The iterative method used to solve the system of linear equations is the biconjugate gradient stabilised solver, or BiCGSTAB(l), developed by Sleijpen and Fokkema (1993). This method has been shown to be one of the most efficient solvers. Further, we increase the solver efficiency by making use of the contraction integral equation described by Zhdanov and Fang (1997) and by Hursan and Zhdanov (2002), instead of using a standard Jacobi pre-conditioner. In our case, the use of a contraction operator is equivalent to solving for $\overline{\overline{a}}\mathbf{E}_a$ instead of solving for $\mathbf{E}_a$ in equation (7), where

$$\overline{\overline{a}} = \frac{2\,\mathrm{Re}\,\sigma_b \overline{\overline{\mathbf{I}}} + \Delta\overline{\overline{\sigma}}}{2\sqrt{\mathrm{Re}\,\sigma_b}}. \tag{16}$$

Accordingly, equation (7) becomes

$$\left(\overline{\overline{\mathbf{I}}} - \overline{\overline{\mathbf{G}}}\overline{\overline{\Delta\sigma}}\right) \cdot \overline{\overline{a}}^{-1} \cdot \left(\overline{\overline{a}} \cdot \mathbf{E}_a\right) = \overline{\overline{\mathbf{G}}}\overline{\overline{\Delta\sigma}} \cdot \mathbf{E}_b. \tag{17}$$

Conceptually, the above equation can be formulated in an iterative manner:

$$\overline{\overline{a}}\mathbf{E}_a^n = C\left(\overline{\overline{a}}\mathbf{E}_a^{n-1}\right), \tag{18}$$

where C is a contraction operator.

Following Zhdanov and Fang (1997), the following inequality remains:

$$\left\| C[\overline{\overline{a}}E_a^{(1)} - \overline{\overline{a}}E_a^{(2)}] \right\| \le \|\beta\|_\infty \left\| \overline{\overline{a}}E_a^{(1)} - \overline{\overline{a}}E_a^{(2)} \right\|, \tag{19}$$

where

$$\|\beta\|_\infty = \max \frac{\left|\overline{\overline{\sigma}} - \sigma_b\right|}{\left|\overline{\overline{\sigma}} + \sigma_b\right|} < 1. \tag{20}$$

The smaller the β, the faster the convergence will be. Applying a similar idea to that of Singer et al. (2002) to the whole domain, an optimal background conductivity can be selected as:

$$\sigma_b = \sqrt{\min\left(\overline{\overline{\sigma}}\right) \cdot \max\left(\overline{\overline{\sigma}}\right)}. \tag{21}$$

With the simultaneous use of both the contraction IE and the optimal background model, an improvement of approximately three fold in numerical performance is achieved compared to that using a standard Jacobi pre-conditioner.

After obtaining $\overline{\overline{a}}\mathbf{E}_a$ from the solution of equation (17), the magnetic field can be calculated at receiver locations using equation (2), in which the total electric field is replaced by

$$\mathbf{E} = \overline{\overline{a}}^{-1}(\overline{\overline{a}}\mathbf{E}_a) + \mathbf{E}_b. \tag{22}$$

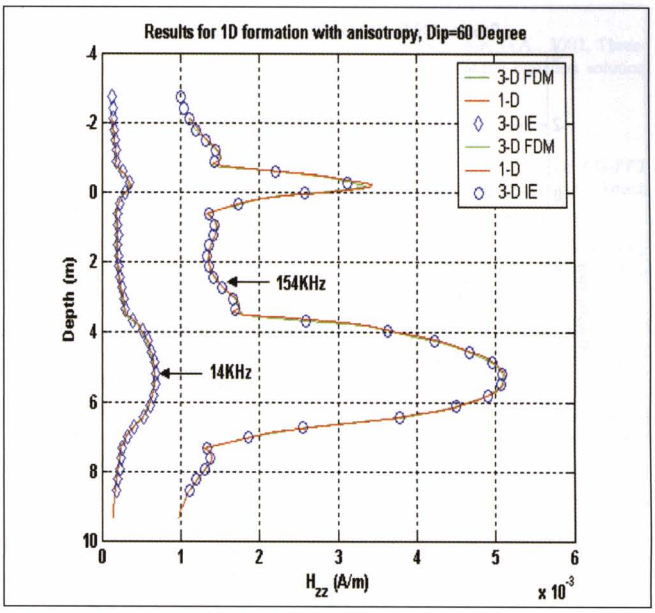

Fig. 3. Comparison of the H_{zz} signal simulated with the new algorithm and a 1D code assuming a 1D formation. The tool and the formation form an angle of 60°. Results for 14 kHz and 154 kHz are shown on this figure.

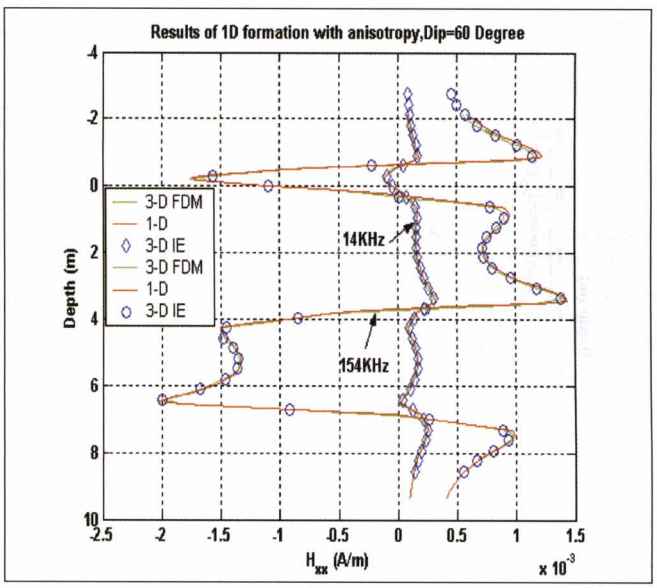

Fig. 4. Comparison of the H_{xx} signal simulated with the new algorithm and a 1D code assuming a 1D formation. The tool and the formation form an angle of 60°. Results for 14 kHz and 154 kHz are shown on this figure.

NUMERICAL VALIDATION

Figure 1 shows the model used in this paper to test the newly developed algorithm. This model was adapted from an example proposed by Wang and Fang (2001) and consists of 5 horizontal layers. The top and bottom layers of the model are isotropic and have a resistivity of 50 Ω·m. The third layer is also an isotropic layer, with a resistivity of 50 Ω·m and a thickness of 14.4 ft. The second and fourth layers are anisotropic with a horizontal resistivity of 3 Ω·m and a vertical resistivity of 15 Ω·m. Thickness of these two layers is 2.4 ft and 12 ft, respectively. Moreover, invasion may exist for these last two layers, with an invasion depth equal to 36 in, and with the resistivity in the invaded zone equal to 3 Ω·m. The borehole has a diameter of 9.6 in. and a resistivity of 1 Ω·m.

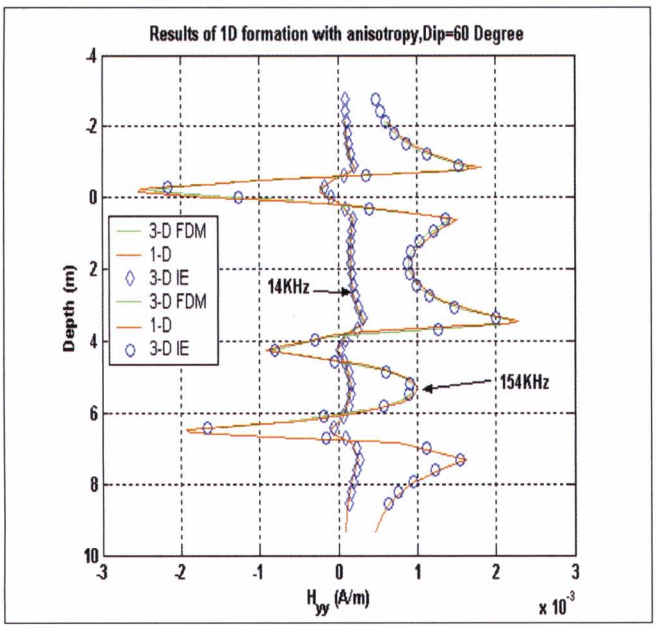

Fig. 5. Comparison of the H_{yy} signal simulated with the new algorithm and a 1D code assuming a 1D formation. The tool and the formation form an angle of 60°. Results for 14 kHz and 154 kHz are shown on this figure.

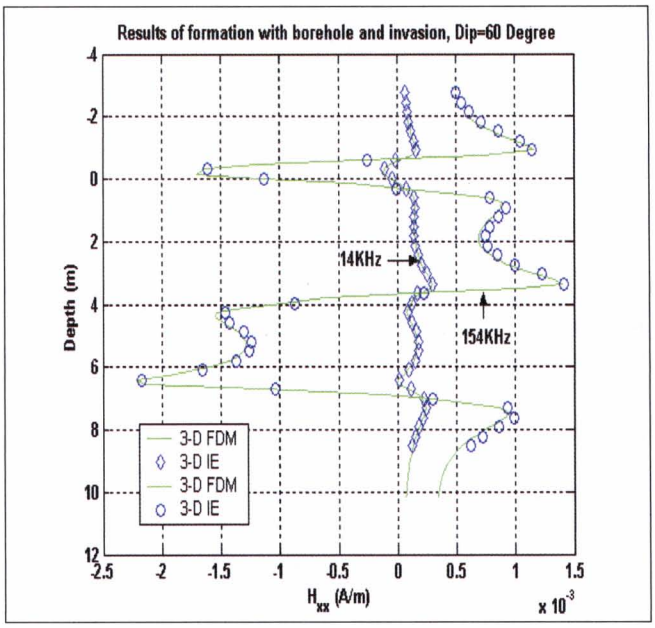

Fig. 7. Comparison of the H_{xx} signal simulated with the new algorithm and a 3D-FDM code assuming a 1D formation with borehole and invasion. The borehole has a dip angle of 60°. Results for 14 kHz and 154 kHz are shown on this figure.

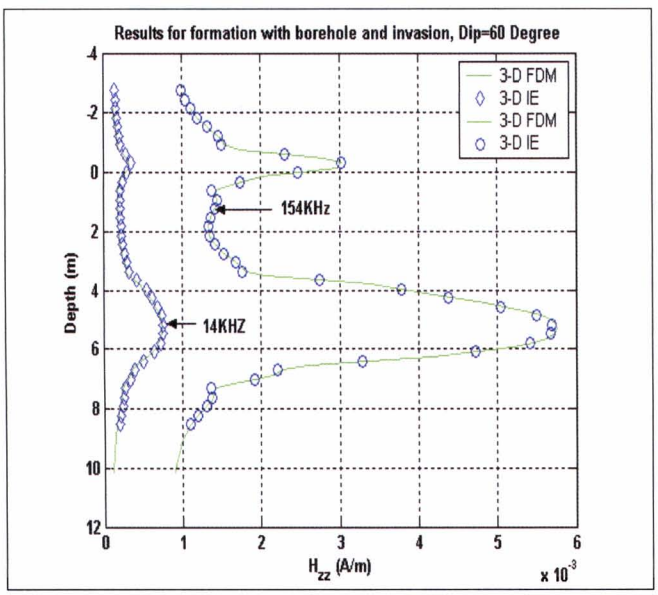

Fig. 6. Comparison of the H_{zz} signal simulated with the new algorithm and a 3D-FDM code assuming a 1D formation with borehole and invasion. The borehole has a dip angle of 60°. Results for 14 kHz and 154 kHz are shown on this figure.

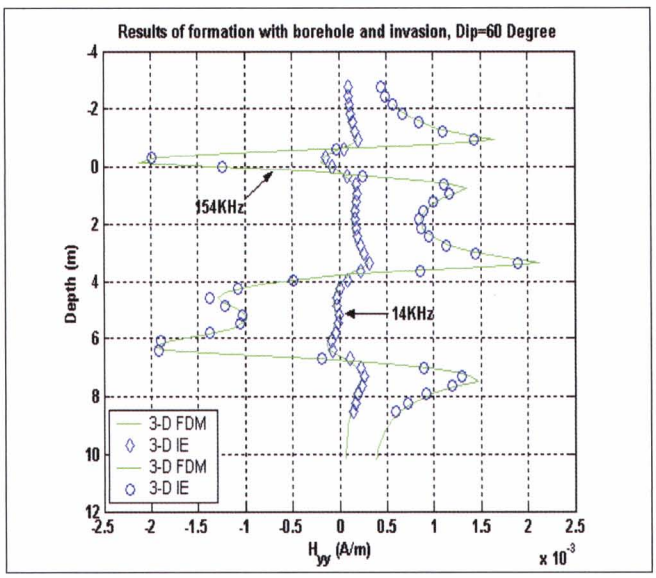

Fig. 8. Comparison of the H_{yy} signal simulated with the new algorithm and a 3D-FDM code assuming a 1D formation with borehole and invasion. The borehole has a dip angle of 60°. Results for 14 kHz and 154 kHz are shown on this figure.

It is also assumed that the borehole may have a dip angle relative to the formation layering. Simulation results are computed for dip angles of 60° for two cases of rock formation model: first, the formation is assumed to exhibit no invasion and no borehole, i.e., it is assumed to consist of a 1D stack of layers. A second model does assume a rock formation with borehole and invasion. Invasion and borehole parameters for this model are as described earlier. We compared simulation results with those provided by 1D code and the 3D Finite Difference Code (**3D FDM** in the figures) written by Wang and Fang (2001). In the descriptions and figures below, the identifier "**3D IE**." refers to the solution developed in this paper.

Figure 2 shows the borehole induction tool configuration assumed in the numerical simulations. It consists of one transmitter and two receivers moving in tandem along the borehole axis. The spacing between the transmitter and the first receiver is 1.2 m (L_1), and the spacing between the transmitter and the second receiver is 1.92 m (L_2). The measurement is assumed to be a combination of the imaginary response in the first receiver (H_1) and the second receiver (H_2), given by the formula

$$H = H_2 - \frac{L_1^3}{L_2^3} H_1 \,. \tag{23}$$

Figures 3–5 show simulation results (H_{zz}, H_{xx}, H_{yy}) obtained with the new algorithm assuming a 1D anisotropy rock formation with a dip angle of 60°. Simulation results for two frequencies (14 kHz and 154 kHz) are compared with those obtained with the 1D code and the finite difference code (3D FDM) developed by Wang and Fang (2001).

Figures 6–8 show simulation results (H_{zz}, H_{xx}, H_{yy}) obtained with the new algorithm assuming a 3D rock formation (borehole and invasion) and a dip angle of 60°. Simulation results for two frequencies (14 kHz and 154 kHz) are compared against those obtained with the 3D FDM code. By comparing Figure 6 with Figure 3, one can visualise borehole and invasion effects for the two simulated frequencies, both in the magnitude and shape of the tool's response.

The above simulation exercises consistently show that the newly developed algorithm yields accurate results in the presence of reasonably complex 3D anisotropy models. A grid size of 128×64×128 was constructed to perform the calculations at 14 kHz. Accordingly, the discretisation in each direction was made uniform and equal to 0.1 m×0.2 m×0.1 m. The average CPU time required for the calculations was approximately 40 minutes per tool location using a 900 MHz Sun Workstation. Simulation of 154 kHz model responses required of a grid size of 64×64×128. The discretisation in all three directions was made uniform with step sizes equal to 0.1 m. These calculations required an average CPU time of approximately 20 minutes per tool location using a 900 MHz Sun Workstation.

CONCLUSIONS

This paper describes a novel integral equation approach for simulating multi-component EM responses in complex 3D conductive media that includes the presence of anisotropy in electrical conductivity. The algorithm assumes a homogeneous and isotropic whole space as the background and uses a uniform discretisation grid in each coordinate direction. Such combination of simulation parameters allows one to take full advantage of the CG-FFT method to efficiently compute and store the entries of the linear system matrix. Furthermore, the use of a contraction integral equation with an optimal background model provides additional efficiency to the computations involved in the novel simulation algorithm. The combined use of the FFT and the iterative linear-system solver BiCGStab(l) makes it possible to approach large-scale simulation problems. Numerical simulations that include more than one million cells can be performed within one hour of CPU time on a 900 MHz Sun Workstation. Benchmark comparisons performed against 1D and 3D finite-difference codes indicate that the new simulation algorithm provides accurate and efficient solutions.

ACKNOWLEDGMENTS

We are obliged to Dr Tsili Wang of Baker Atlas for many useful discussions and for providing finite-difference simulation results used for some of the test model examples described in this paper. The technical support of Dr D. Georgi and Dr L. Tabarovsky during the development of this project is highly appreciated. Finally, a note of gratitude goes to Baker Atlas for permission to publish the results of this work.

REFERENCES

Avdeev, D.B., Kuvshinov, A.V., Pankratov, O.V., and Newman, G.A., 2002, Three-dimensional induction logging problems, Part 1: An integral equation solution and model comparisons: *Geophysics*, **67**, 413–426.

Born, M., 1933, *Optics*: Springer-Verlag.

Catedra, M.F., Torres, R.P., Basterrechea, J., and Gago, E., 1995, *The CG-FFT method: Application of signal processing techniques to electromagnetics*: Artech House.

Fang S., and Wang, T., 2000, Accurate Born simulation of induction response using an optimal background: *70th Annual International Meeting, Society of Exploration Geophysicists, Expanded Abstracts*, 1806–1809.

Gan, H., and Chew, W.C., 1994, *A discrete BCG-FFT Algorithm for Solving 3D inhomogeneous Scatterer Problems:* Electromagnetic Laboratory, Department of Eletrical and Computer Engineering, University of Illinois.

Gao, G-Z., Fang, S., and Torres-Verdín, C., 2003, A New Approximation for 3D Electromagnetic Scattering in the Presence of Anisotropic Conductive Media: *3DEM-III Symposium, Adelaide, Australia.*

Gianzero, S., 1999, The paradox of anisotropy revisited: *The Log Analyst*, **40**, 485–491.

Golub, G.H., and Van Loan, C.F., 1996, *Matrix Computations, Third edition*: The Johns Hopkins University Press.

Habashy, T.M., Groom, R.W., and Spies, B., 1993, Beyond the Born and Rytov approximations: A nonlinear approach to electromagnetic scattering: *Journal of Geophysical Research*, **98**, 1759–1775.

Hohmann, G.W., 1983, Three-dimensional EM modelling: *Geophysical Surveys*, **6**, 27–53.

Hursan, G., and Zhdanov, M.S., 2002, Contraction integral equation method in three-dimensional electromagnetic modeling: *Radio Science*, **37**, 1–13.

Klein, J.D., Martin, P.R., and Allen, D.F., 1997, the petrophysics of electrically anisotropic reservoirs: *The Log Analyst*, May-June.

Kriegshauser B., Fanini, O., and Yu, L., 2000, Advanced inversion techniques for multicomponent induction data: *Presented at the 70th Annual International Meeting, Society of Exploration Geophysicists.*

Liu, Q.H., Zhang, Z.Q., and Xu, X.M., 2001, The hybrid extended Born approximation and CG-FFT method for electromagnetic induction problems: *IEEE Transactions on Geoscience and Remote Sensing*, **39**(2).

Moran, J.H., and Gianzero, S., 1979, Effects of formation anisotropy on resistivity-logging measurements: *Geophysics*, **44**, 1266–1286.

Newman, G.A., and Alumbaugh D.L., 2002, Three-dimensional induction logging problems, Part 2: A finite-difference solution for 3-D induction logging problems: *Geophysics*, **67**, 484–491.

Singer, B.Sh., Mezzatesta, A., and Wang, T., 2002, 3D modelling of electromagnetic field in subsurface and borehole environments: *72nd Annual International Meeting, Society of Exploration Geophysicists, Expanded Abstracts*, 312–315.

Sleijpen, G.L.G., and Fokkema, D.R., 1993, BiCGSTAB(l) for Linear Equations Involving Unsymmetric Matrices with Complex Spectrum: *Electronic Transactions on Numerical Analysis*, **1**, 11–32.

Wang T., and Fang S., 2001, 3-D electromagnetic anisotropy modeling using finite differences: *Geophysics*, **66**, 1386–1398.

Wannamaker, P.E., Hohmann, G.W., and SanFilipo, W.A., 1983, Electromagnetic modelling of three-dimensional bodies in layered earths using integral equations: *Geophysics*, **49**, 60–74.

Xiong, Z., 1992, Electromagnetic modeling of 3-Dstructures by the method of system iteration using integral equations: *Geophysics*, **57**, 1556–1561.

Xiong, Z., and Tripp, A.C., 1995, Electromagnetic scattering of large structures in a layered earth using integral equations: *Radio Science*, **30**, 921–929.

Zhdanov, M.S., and Fang S., 1996, Quasi-linear approximation in 3-D electromagnetic modeling: *Geophysics*, **61**, 646–665.

Zhdanov, M.S., and Fang S., 1997, Quasi-linear series in three-dimensional electromagnetic modeling: *Radio Science*, **32**, 2167–2188.